Research Article Open Access

Wenxing Zheng and Xinhou Wang*

Effects of cylindrical-electrode-assisted solution blowing spinning process parameters on polymer nanofiber morphology and microstructure

https://doi.org/10.1515/epoly-2019-0020
Received September 27, 2018; accepted November 07, 2018.

Abstract: Cylindrical-electrode-assisted solution blowing spinning (CSBS) is a novel method for preparing polymer nanofibers by using air-stretch and electrostatic simultaneously, which can fabricate thinner and more uniform nanofibers than the traditional solution blowing spinning (SBS). In this work, the effects of processing parameters including length of cylinder (LC), needle to cylinder distance (NCD) and left face of cylinder to collector distance (CCD) on the CSBS nanofiber diameter were investigated. The results are as follows: when the NCD decreased, the fiber diameter decreased; when the LC increased, the fiber diameter decreased; the CCD didn't significantly affect the fiber diameter. Moreover, an orthogonal experimental design was utilized to investigate the effect of injection rate, air pressure, NCD, LC, diameter of cylinder (DC), voltage and CCD on the fiber diameter and porosity of various surface layers of nanofiber web (P1, P2, and P3). The results showed that the varied range of each properties (average diameter, standard deviation of the diameter, P1, P2, and P3) was 539.121-904.149 nm, 127.903-303.253, 71.464-85.1415%, 60.32725-75.46625%, 48.23925-70.08875%, respectively. We also found the order of the influence of the above-mentioned seven process parameters on each above properties of the nanofiber web, and the corresponding optimal spinning process parameters were listed. It is well known that the fiber diameter affects the mechanical properties of nanofibers, and porosity of nanofiber webs is an important parameter in tissue engineering, bioengineering, and filtration. The effects of CSBS process parameters on nanofiber morphology and microstructure were investigated for the first time. The conclusion of the paper can help researchers to produce high quality CSBS nanofiber and promote the wider application of this novel technology.

Keywords: cylindrical-electrode-assisted solution blowing spinning; parameters study; polymer nanofiber; electrostatic induction; morphology

1 Introduction

Solution blowing spinning (1) (SBS) has attracted wide interest over the past ten years due to its versatility and high productivity. The throughput of SBS can be 10 times larger than electrospinning's (1-3). SBS uses high pressure air as the stretching force of fiber formation. The nanofibers prepared by SBS have been used in biomedical applications (4-6), filtration applications (7,8), energy applications (9-14). However, the nanofibers fabricated by the SBS have some inevitable defects, such as more slag balls, larger fiber diameter and bad continuity (15,16).

In our previous research, a novel spinning method called cylindrical-electrode-assisted solution blowing spinning (CSBS) was invented. The CSBS technique prepares nanofibers by using electrostatic forces and air-stretch simultaneously. The structures of nanofiber mats fabricated by the CSBS were similar to SBS ones. However, compared with SBS fibers, the CSBS fiber's diameter standard deviation (SD) decreased by 21% and the fiber mean diameter decreased by 6.17%. The thinner and more uniform fibers made the CSBS fiber web more fits for filtration and other uses compared with the solution blowing spinning one (17). CSBS has different spinning mechanisms from traditional electrospinning. In the electrospinning system, the jet is connected to a power source, and the jet is directly charged by the power source (18-20). But, in the CSBS system, the jet is charged due to the action of electrostatic induction.

* **Corresponding author: Xinhou Wang,** College of Textiles, Donghua University, Shanghai, 201620, P.R. China, e-mail: xhwang@dhu.edu.cn
Wenxing Zheng, College of Textiles, Donghua University, Shanghai, 201620, P.R. China, College of Light Industry and Textile, Qiqihar University, Qiqihar, 161000, P.R. China.

However, the previous literature only describes the apparatus of the CSBS and the advantages of this spinning method, but lacks the study of the process parameters of the CSBS. The questions that need further study are as follows: Which process parameters are adjustable, how these process parameters will affect the properties of the nanofibers, and how much the various parameters affect nanofiber performance? Solving the above problems is more conducive to the application of the technology in various related fields.

In this study, we have systematically researched the effects of main process parameters, including LC, NCD and CCD on the nanofiber diameter of CSBS PEO fibers. Furthermore, an orthogonal test was designed to research the effects of more process parameters (injection rate, air pressure, NCD, LC, DC, voltage and CCD) on the fiber diameter and porosity of various layers of nanofiber web. The first systematic study of these parameters can help researchers better understand and utilize the CSBS technology and promote the application of this new technology in various fields.

2 Experimental

2.1 Materials

Polyethylene oxide (PEO) with an average Mw of 10^6, was purchased from Shanghai Liansheng Chemical Co., Ltd (China). The PEO solution (viscosity≈23,800mPa.S) was prepared by dissolving PEO powder in the distilled water to prepare the solution at 7 wt% concentration. The mixture was stirred by using a magnetic stirrer at room temperature for 24 h. Then the mixture was left to rest for 10 h.

2.2 Equipment and process

The schematic of CSBS setup was illustrated in Figure 1. It consists of (A) high pressure air compressor, (B) custom-made die, (C) injection pump, (D) hypodermic syringe, (E) needle, (F) custom-made hollow metal cylinder, (G) high voltage power, and (G) grounded metal receiver.

The spinning solution was delivered to the needle (the inner diameter of the needle was 0.42 mm) (E) by adjusting the micro-syring pump (C) at different flow rate. The high-velocity air was supplied to the home-made die (B) by adjusting the compressor (A) at different pressure. The spinning solution droplet at the tip of the needle (E) was stretched by the high-velocity air which blown from the custom-made die (B) and flew to the collector (H). The cylindrical electrode (F) is connected to the power source (G), and an electrostatic field is formed around the cylindrical electrode (F) when the power source (G) is worked. When the flying jet approaches the cylindrical electrode (F), the jet will be charged in the electrostatic field due to the electrostatic induction effect. Different electric field intensity can be obtained via controlling the voltage of the high voltage source (G). The solution stream was attenuated to nanofibers by utilizing electrostatic forces and air-stretch simultaneously.

2.3 Investigation of main influencing processing parameters

2.3.1 Single factor design

In this study, the processing parameters of CSBS including length of cylinder (LC), needle to cylinder distance (NCD), and left face of cylinder to collector distance (CCD) were chosen to study the impact of these parameters on the diameter of PEO nanofiber. Each of the aforementioned three factors was changed at five levels while all other factors unchangeable. The spinning conditions for each single-factor experiment were listed in Tables 1-3.

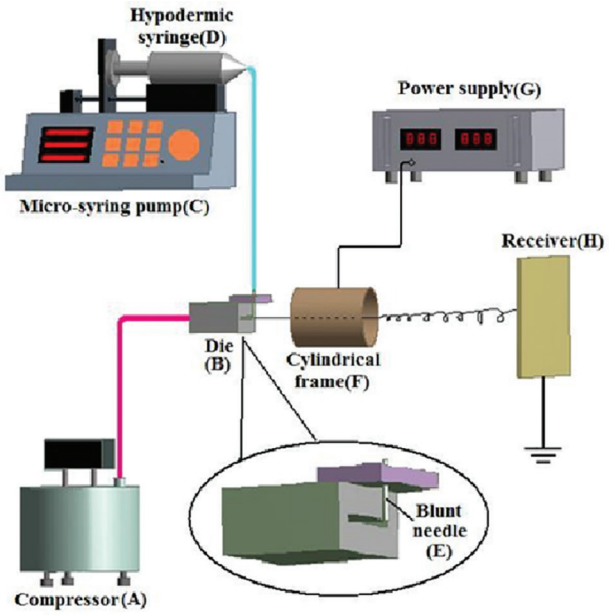

Figure 1: The schematic of cylindrical-electrode-assisted solution blowing spinning (CSBS) setup (17).

Table 1: Spinning conditions of different NCD.

Parameter	Values
Voltage (kV)	10
Length of cylinder (LC) (cm)	10
Diameter of cylinder (DC) (cm)	15
Needle to cylinder distance (NCD) (cm)	5,10,15,20,25
Left face of cylinder to collector distance (CCD) (cm)	75
Feed rate (ml/h)	0.2
Air pressure (MPa)	0.01

Table 2: Spinning conditions of different LC.

Parameter	Values
Voltage (kV)	10
Length of cylinder (LC) (cm)	6,8,10,12,14
Diameter of cylinder (DC) (cm)	15
Needle to cylinder distance (NCD) (cm)	5
Left face of cylinder to collector distance (CCD) (cm)	95
Feed rate (ml/h)	0.5
Air pressure (MPa)	0.01

Table 3: Spinning conditions of different CCD.

Parameter	Values
Voltage (kV)	10
Length of cylinder (LC) (cm)	10
Diameter of cylinder (DC) (cm)	15
Needle to cylinder distance (NCD) (cm)	5
Left face of cylinder to collector distance (CCD) (cm)	75,80,85,90,95
Feed rate (ml/h)	0.2
Air pressure (MPa)	0.01

2.3.2 Orthogonal design

In this paper, the effects of seven factors on the CSBS nanofibers diameter and the porosity of various layers were studied by orthogonal analysis. These seven factors were: air pressure, voltage, length of cylinder (LC), diameter of cylinder (DC), injection rate, needle to cylinder distance (NCD), and left face of cylinder to collector distance (CCD). Two levels of every factor were tested as listed in Table 4.

Table 4: The details of factors and their levels for orthogonal experimental design.

Factor	Level1	Level2
Air pressure (MPa)	0.01	0.015
Voltage (kV)	7	10
Length of cylinder (LC) (cm)	10	14
Diameter of cylinder (DC) (cm)	15	20
Injection rate (ml/h)	0.3	0.2
Needle to cylinder distance (NCD) (cm)	15	5
Left face of cylinder to collector distance (CCD) (cm)	85	95

2.4 Morphology and microstructure analysis

Uncovered all the samples from the collector. The morphologies of cylindrical-electrode-assisted solution blowing spinning nanofibers were observed by scanning electron microscopy (SEM; Hitachi S-3400, High-Technologies, Japan). Each fiber nonwoven was coated with a gold layer.

The diameter of the nanofiber and the porosity of the various layers of nanofiber web were measured using image analysis software (Image J, USA). Four SEM photographs were taken from each sample. At least 60 random measurements from the 4 SEM photos have been measured for each sample to determine the PEO nanofiber diameter. Each of the SEM photos was converted to binary images using different thresholds to calculate the porosity of the different layers of the nanofiber web. Details of this porosity measurement method have been described in the literature of Ghasemi-Mobarakeh et al. (21).

3 Results and discussion

3.1 Effects of processing parameters on the diameter of fiber

3.1.1 Effect of the needle to cylinder distance (NCD) on the fiber diameter

The needle to cylinder distance (NCD) was an important parameter in the CSBS process. Figures 2a-e illustrate SEM photos of PEO nanofibers fabricated at NCD of 5, 10, 15, 20, 25 cm, respectively. The dependence of the fiber diameter on NCD was shown in Figure 2f. As shown in Figure 2f, when the NCD was increased from 5 to 25 cm, the average diameter increased from 570.976 to 787.073 nm. In CSBS process, when the flying spinning jet which sprayed from the needle approaches the cylinder, the jet will be charged due to electrostatic induction effect. The evaporation of solvent and air stretching reduces the thickness of the jet and increases the surface charge density of the jet. The increased density of surface

charge splits the solution jet to thinner jets due to mutual charge repulsion. This procedure may repeat many times to decrease the fiber diameter (17,22). It is known from electrical knowledge that the electric field strength is greater as it is closer to the charged body. Conversely, the farther away from the charged body, the electric field strength is small. A smaller NCD means that the distance between the needle tip and the electrode is smaller. Therefore, the electric field strength at the tip of the needle is large when the NCD is small. Since the jet is ejected from the tip of the needle, the electric field intensity around the jet is larger as the NCD is smaller. At this time, the electrostatic induction effect of the jet is more obvious. This results in a greater induced charge density on the jet. An increase in the jet charge density results in an increase in the splitting frequency of the spinning jet, and finally, decreases the nanofiber diameter (17,22). In addition, reducing the NCD causes the jet to enter the electric field in the cavity of the electrode earlier, thereby charging earlier in the electric field in the electrode's cavity. This is also one of the reasons for the fiber to become finer.

3.1.2 Effect of length of cylinder (LC) on the fiber diameter

One of the major originalities of CSBS has lain in adding the charged cylinder. So it's necessary to investigate the impact of cylinder length on the fiber diameter. Figures 3a-e show SEM images of spun nanofiber at LC of 6, 8, 10, 12, 14 cm, respectively. The relationship between LC and the fiber diameter is illustrated in Figure 3f. As depicted in Figure 3f, when the LC was increased from 6 to 14 cm, the average diameter decreased from 1354.209 to 1184.889 nm. The following is the possible explanation for the above result: an increase LC can increase the time of solution jet pass through the cylinder. The increase in the time it takes for the jet to pass through the cylinder extends the duration of the electrostatic induction effect, causing the jet to charge more fully due to electrostatic induction effects. For the above reasons, the splitting frequency of the jet increases, eventually making the fiber diameter smaller. During the course of the experiments, we found that too large LC is not conducive to the jet flow through the cylindrical electrode.

3.1.3 Effect of left face of cylinder to collector distance (CCD) on the fiber diameter

Figures 4a-e illustrate SEM images of nanofiber mats prepared at CCD of 75, 80, 85, 90, 95 cm, respectively. Figure 4f shows the relationship between CCD and the fiber diameter. As shown in Figure 4f, when the CCD was increased from 75 to 95 cm, the average diameter of PEO fibers could be varied in a very narrow range of 572.8425 to 613.4979 nm. That is to say, the influence of CCD on the fiber diameter was not obvious. In the CSBS process, the solution jets were stretched by electrostatic force plus air shearing force (17). Intuitively, increasing the CCD means increasing the distance the jet flies, which in turn increases the jet flight time. In longer flight times, the jet will be stretched more fully by the airflow pull and electrostatic forces, which will result in a smaller fiber diameter.

However, the effective air stretching distance is very short (≈100μm) from the injection nozzle (23,24). Increase CCD couldn't improve the effect of air-stretch. Medeiros et al also found the working distance did not have significant effect on the fiber diameter when nanofibers obtained by solution blowing spinning system (1). During the CSBS process, the solution jet will solidify into fiber due to solvent evaporation. The solidification of the jet increase the viscosity of the jet, which in turn increase the surface tension of the jet. When the surface tension of the jet exceeds the repulsive electric force of spinning jet, the splitting of jets ended. When the above situation occurs, only increasing the CCD without changing the other parameters will not affect the frequency of the splitting. That is to say, in a certain range, enhancement of CCD couldn't increase the splitting frequency. Chang Seok Ki et al also found the effect of spinning distance (SD) on the size of nanofibers was not significant when nanofibers were prepared by electrospinning system (25). In the course of the experiments, we also found that an excessively large CCD is not conducive to the accumulation of nanofibers on the receiver. This is because the increase of the CCD leads to an increase in the distance of the jet flight, which in turn causes an increase in the divergence of the airflow, which is not conducive to the reception of the nanofiber. However, too short CCD may produce bead defects, and cause fibers adhere to each other due to not enough distance was provided for evaporation of solvent.

3.2 Analysis of experimental parameters via orthogonal design

3.2.1 Morphology of CSBS nanofibers

The process variables of SBS are few (26). However, the process parameters of CSBS are more than SBS. Thus, it is important to research the effects of these process parameters on the fiber diameter and nanofiber web

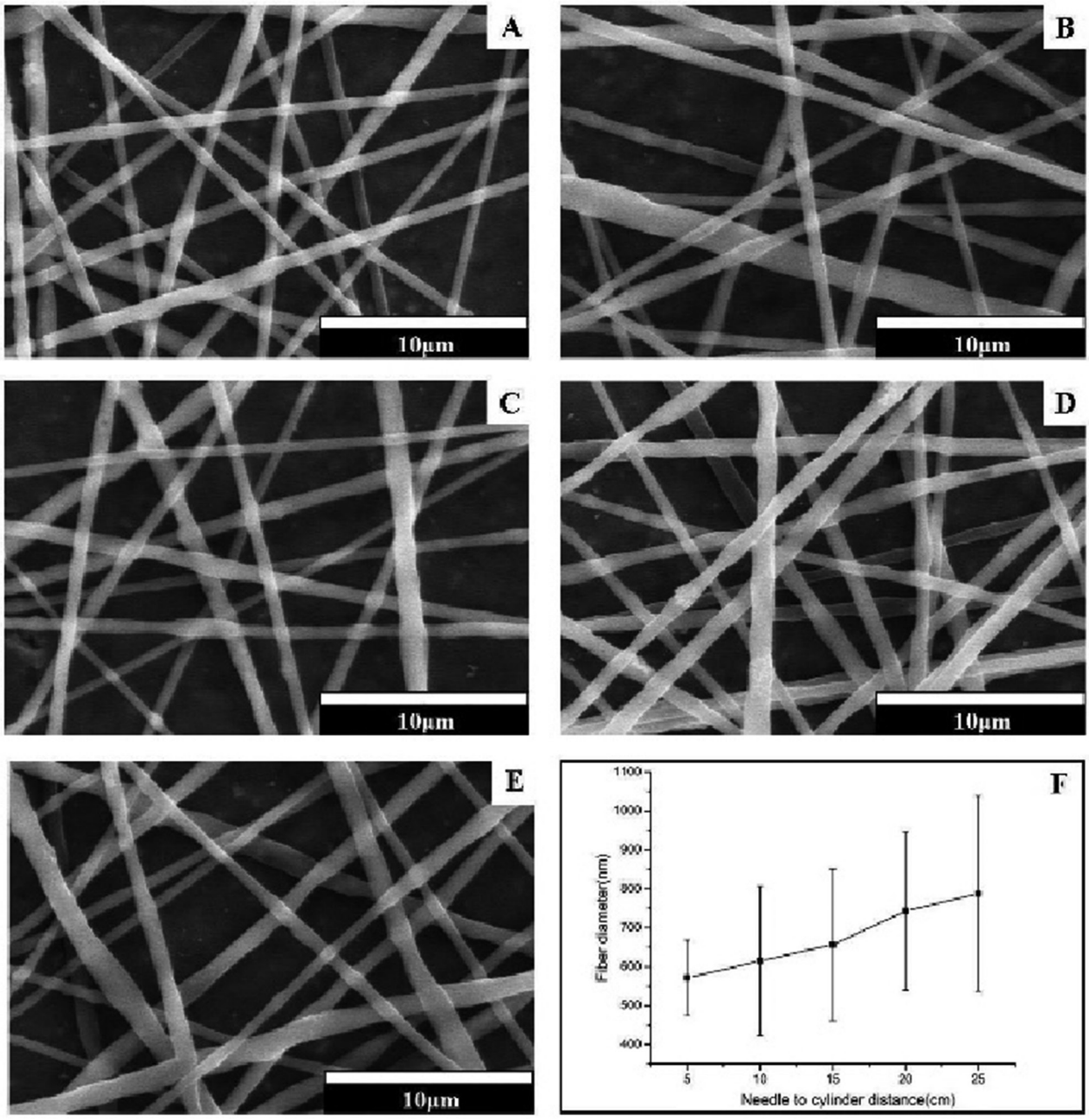

Figure 2: SEM photos of nanofibers prepared by CSBS system at the NCD: (a) 5 cm, (b) 10 cm, (c) 15 cm, (d) 20 cm, (e) 25 cm, (f) relationship between NCD and the fiber diameter.

porosity in the CSBS process. The orthogonal array design plan, the average fiber diameter, the standard deviation of the fiber diameter, and the different layers' porosity (P1, P2, P3) for each experiment were shown in Table 5. SEM photos of CSBS PEO nanofibers correspond with experiments list in Table 5 were shown in Figure 5.

As showed in Table 5, where M_{ij} indicate the sum of each fiber morphology or microstructure properties indexes values (including the average fiber diameter, fiber diameter standard deviation, P1, P2, and P3) of row "j" if the level is i. R_j represents the difference between the M_{1j} value and the M_{2j} value in the "j" column. A large R_j value indicated the effect of the factor j on this corresponding properties index was significant. From Table 5, the R_j values of the fiber average diameter corresponding to each factor range from 484.025>483.477>439.519>324.417>248.885>53.091>37.583. Thus, the importance order of the seven factors on the nanofiber average diameter can be listed as follows: injection rate>air pressure>NCD>DC>LC>voltage>CCD.

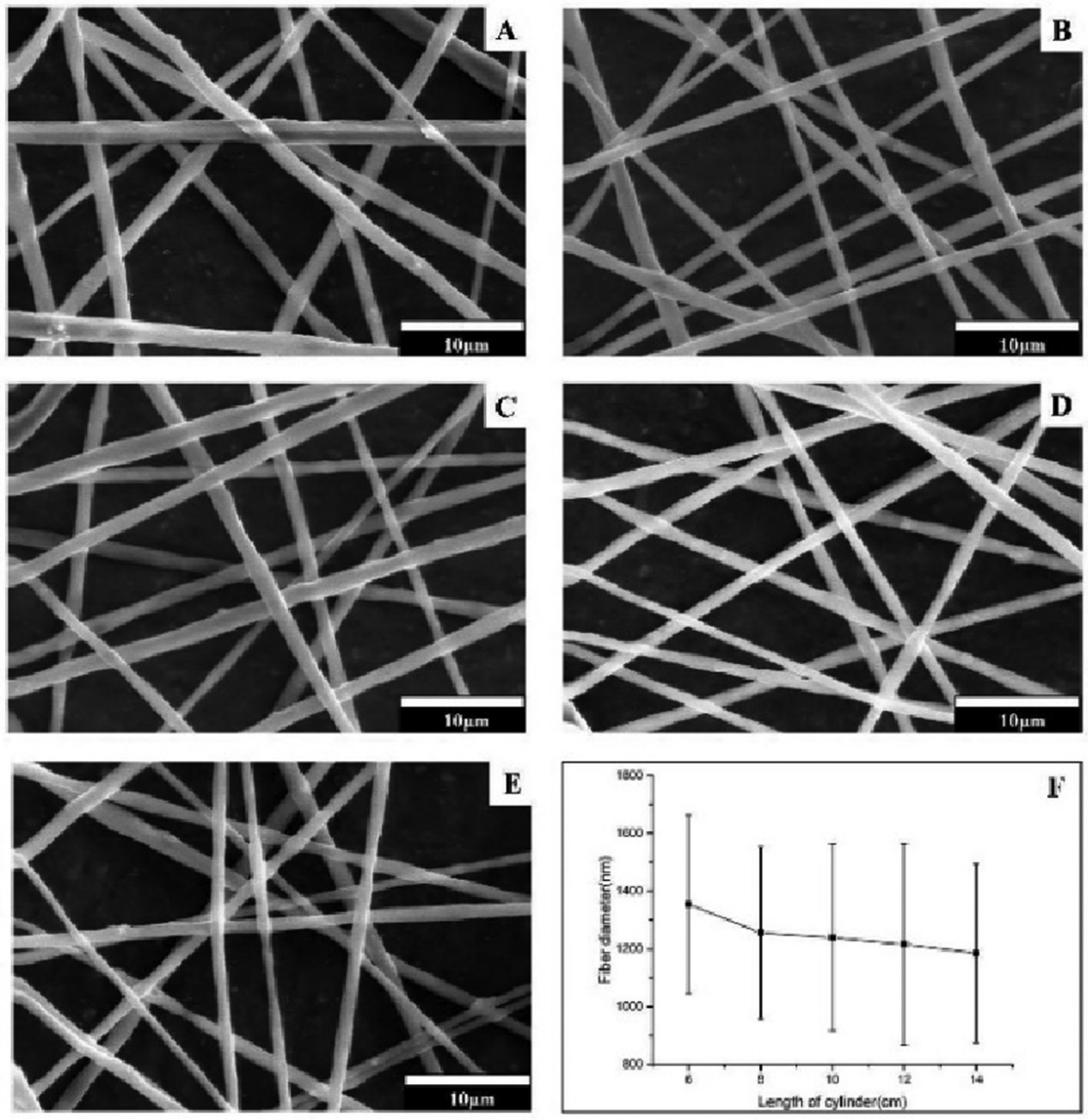

Figure 3: SEM images of nanofiber nonwoven produced by CSBS at the LC: (a) 6 cm, (b) 8 cm, (c) 10 cm, (d) 12 cm, (e) 14 cm, (f) relationship between LC and fiber diameter.

Similarly, the importance order of each factor on the fiber diameter standard deviation was as follows: NCD>DC>voltage>CCD>LC>air pressure>injection rate. The R_j value of the fiber average diameter corresponding to CCD was 37.583, which was the smallest of all seven process parameters. This means that the CCD has no significant effect on the average fiber diameter. This conclusion is consistent with the conclusions in Section 3.1.3 of this paper. Table 5 also indicated that the average diameter and standard deviation of the diameter varied from 539.121 to 904.149 nm and 127.903 to 303.253 nm, respectively.

As can be seen from Figure 5 and Table 5, the nanofibers prepared in Experiment 7 had the smallest fiber diameter and the best diameter uniformity. According to Table 5, injection rate, air pressure and NCD were the three most important factors affecting the average diameter of fibers, the R_j values of these three process parameters were much larger than other parameters. In all of the eight

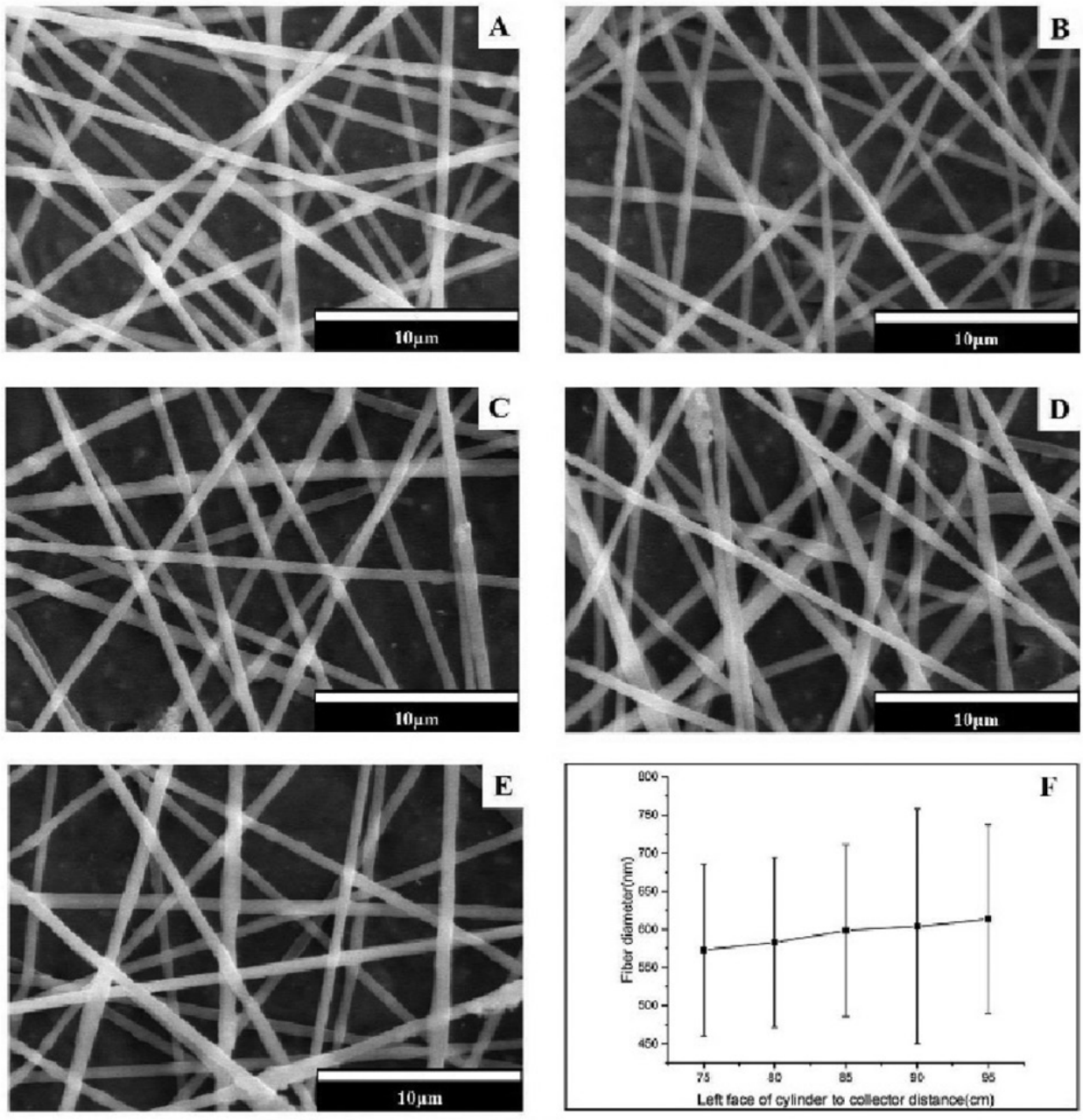

Figure 4: SEM photos of PEO nanofiber mats obtained by CSBS at the CCD: (a) 75 cm, (b) 80 cm, (c) 85 cm, (d) 90 cm, (e) 95 cm (f) relationship between CCD and fiber diameter.

experiments, Experiment 7 had the highest air pressure, the lowest injection rate, and the smallest NCD. According to the conclusions in Section 3.1.1 and references (1,27), reducing the injection rate or increasing the gas pressure or reducing NCD leads to a decrease in nanofiber diameter. Therefore, the fiber diameter of Experiment 7 was the smallest.

It is known that the fiber diameter could affect the mechanical properties of nanofiber (28), nanofiber web pore size and other properties. Therefore, the conclusions of this paper can be applied to many applications of CSBS nanofibers.

3.2.2 Porosity of various layers of CSBS nanofiber web

After converting the SEM images to binary form by using ImageJ, different thresholds can be used to observe the various layers of nanofiber web. The

Table 5: Effect of seven parameters on the average fiber diameter, fiber diameter standard deviation, P1, P2, and P3.

Experiment		Air pressure (MPa)	Voltage (kV)	LC (cm)	DC (cm)	Injection rate (ml/h)	NCD (cm)	CCD (cm)	Average diameter (nm)	SD of fiber diameter	P1 (%)	P2 (%)	P3 (%)
1		1	1	1	1	1	1	1	904.149	262.385	81.5695	72.689	68.593
2		1	1	1	2	2	2	2	763.763	281.317	82.79225	71.1785	64.83775
3		1	2	2	1	1	2	2	728.171	168.6	84.4715	64.98425	48.23925
4		1	2	2	2	2	1	1	788.753	243.283	76.31075	66.30825	61.27975
5		2	1	2	1	2	1	2	609.448	268.72	85.1415	75.46625	70.08875
6		2	1	2	2	1	2	1	692.283	218.281	76.4795	65.4595	59.49125
7		2	2	1	1	2	2	1	539.121	127.903	78.8675	64.47925	50.15
8		2	2	1	2	1	1	2	860.507	303.253	71.464	60.32725	56.51425
Average diameter (nm)	M_{1j}	3184.836	2969.643	3067.54	2780.889	3185.11	3162.857	2924.306					
	M_{2j}	2701.359	2916.552	2818.655	3105.306	2701.085	2723.338	2961.889					
	R_j	483.477	53.091	248.885	324.417	484.025	439.519	37.583					
SD of fiber diameter	M_{1j}	955.585	1030.703	974.858	827.608	952.519	1077.641	851.852					
	M_{2j}	918.157	843.039	898.884	1046.134	921.223	796.101	1021.89					
	R_j	37.428	187.664	75.974	218.526	31.296	281.54	170.038					
P1 (%)	M_{1j}	325.144	325.9828	314.6933	330.05	313.9845	314.4858	313.2273					
	M_{2j}	311.9525	311.1138	322.4033	307.0465	323.112	322.6108	323.8693					
	R_j	13.1915	14.869	7.71	23.0035	9.1275	8.125	10.642					
P2 (%)	M_{1j}	275.16	284.7933	268.674	277.6188	263.46	274.7908	268.936					
	M_{2j}	265.7323	256.099	272.2183	263.2735	277.4323	266.1015	271.9563					
	R_j	9.42775	28.69425	3.54425	14.34525	13.97225	8.68925	3.02025					
P3 (%)	M_{1j}	242.9498	263.0108	240.095	237.071	232.8378	256.4758	239.514					
	M_{2j}	236.2443	216.1833	239.099	242.123	246.3563	222.7183	239.68					
	R_j	6.7055	46.8275	0.996	5.052	13.5185	33.7575	0.166					

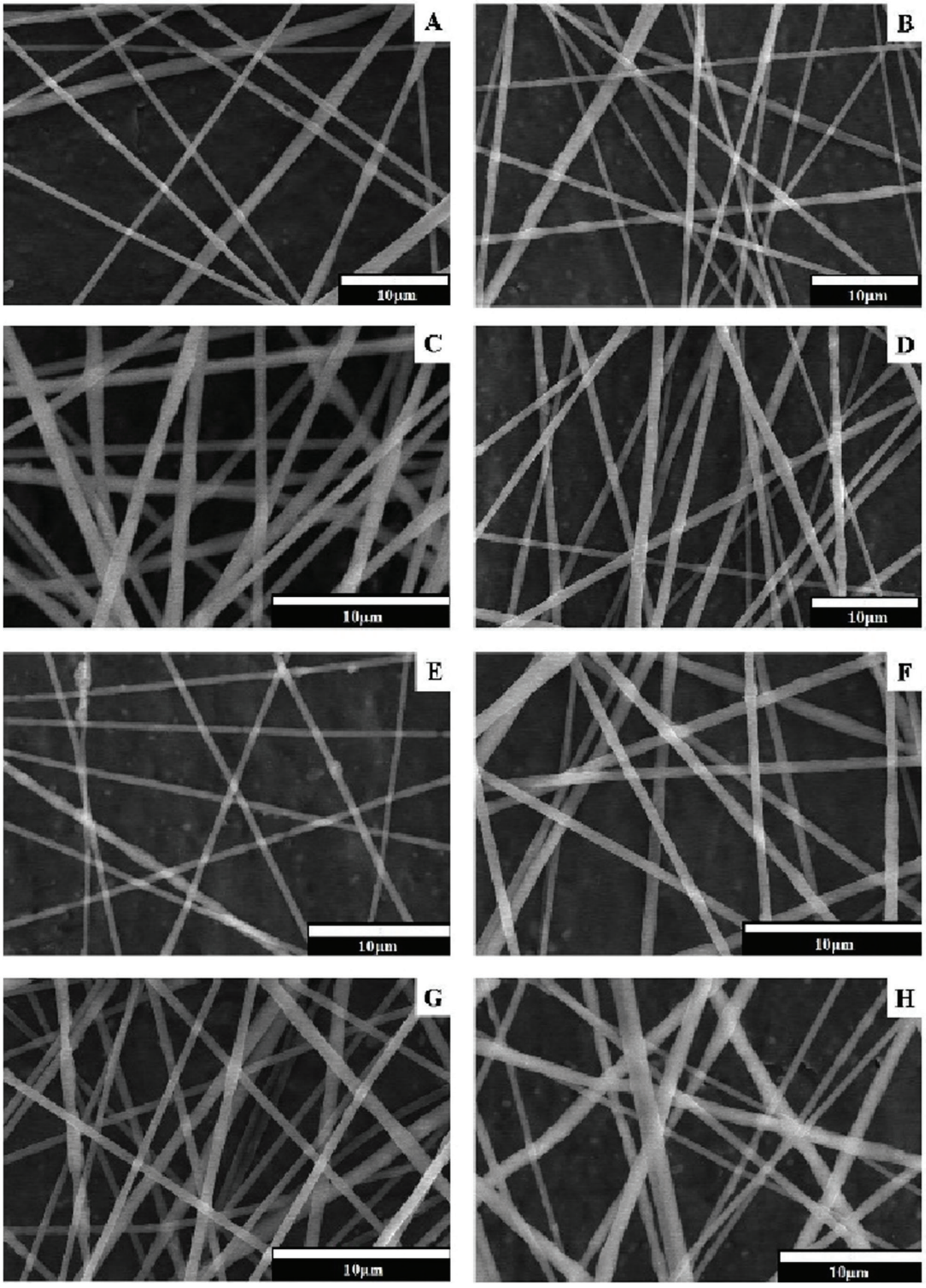

Figure 5: SEM photos illustrating the morphology of the PEO nanofiber mats: (a-h) correspond to Experiments 1-8.

magnifications of Experiments 3, 6, and 7 were 5000×, the magnifications of Experiments 5 and 8 were 4000×, and the magnifications of Experiments 1, 2, and 4 were 3000×. Figure 6 shows the histogram of different images with different magnification. As it can be seen in Figure 6, SEM images of different magnifications had different histograms. However, as described by Ghasemi-Mobarakeh et al. (21), the results of the method used herein did not depend upon the histogram or magnification of the images. This method can be used to calculate different layers' porosity from most of images histogram and magnifications.

Figure 7 shows the different binary images of the no. 7 experiment under various thresholds. The morphologies of the various layers of the nanofiber web were shown by the selection of different thresholds. When threshold 1 was applied, only the surface layer appeared in the binary image. By applying threshold 2, the surface and the middle layer were displayed. When the threshold was 3, all layers of the nanofiber web can be seen.

After converting the each original image into different binary images, the each binary image's porosity was calculated using Eq. 1:

$$P = \left(1 - \frac{n}{N}\right) \times 100 \tag{1}$$

where N is the total number of pixels in the binary image, n is the number of white pixels, and P is the porosity of each binary image. The porosity of binary images with thresholds of 1, 2 and 3 were presented as P1, P2 and P3, respectively. The calculation results of the porosity of different layers of each sample in the orthogonal experiment were shown in Table 5. Four SEM photographs were taken for each sample, and each of the porosity values in Table 5 was the average porosity values of the four SEM photographs.

The results in Table 5 show that the R_j values of the P1 corresponding to each factor range from 23.0035>14.869>13.1915>10.642>9.1275>8.125>7.71. Thus, the importance order of the seven process parameters on P1 can be listed as follows: DC>voltage>air pressure>CCD>injection rate>NCD>LC. Similarly, the importance order of each factor on P2 was: voltage>DC>injection rate>air pressure>NCD>LC>CCD. The importance order of seven factors on P3 was as follows: voltage>NCD>injection rate>air pressure>DC>LC>CCD.

As shown in Table 5, the varied range of P1, P2, and P3 was 71.464-85.1415%, 60.32725-75.46625%, 48.23925-70.08875%, respectively. The P1, P2, and P3 values of Experiment 5 were the largest, which indicates that the porosity of the different layers of Experiment 5 was the largest. Both P1 and P2 values of Experiment 8 were the smallest. This means that the porosity of the first and second layers of Experiment 8 was the smallest. The P3 values of Experiment 3 and Experiment 7 were approximately equal and smaller than the P3 values of the other experiments. The reason was followed: it can be seen from Table 5 that voltage and NCD were the parameters that had the greatest influence on P3, and their R_j values were much larger than other parameters. The voltage and NCD of Experiment 3 and Experiment 7 had the same value,

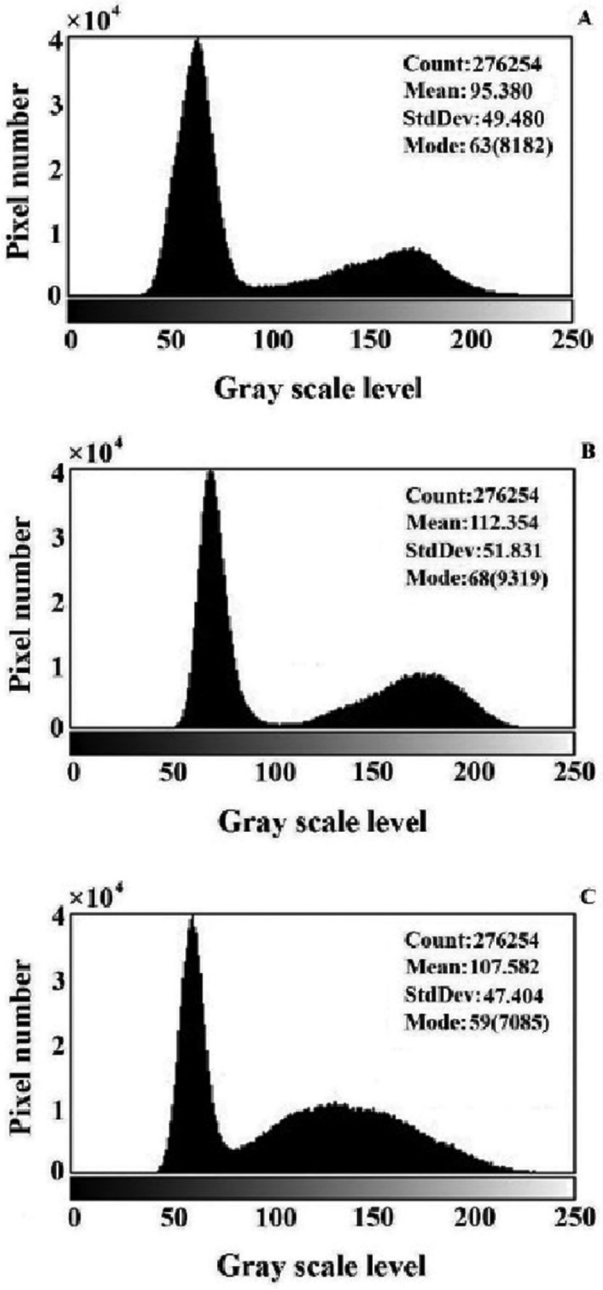

Figure 6: Histogram of different SEM photos. Magnification of (a) 3000, (b) 4000 and (c) 5000.

so their P3 values were approximately equal. Although the P3 values of Experiment 3 and Experiment 7 were not significantly different, it can be seen from Figure 5 that the morphologies of the pores of these two experiments were different, the pores of Experiment 3 were larger than that of Experiment 7. The reason is that the larger diameter fibers formed larger pores than those formed by smaller diameter fibers (29). It also can be seen from Figure 5 that the number of pores in Experiment 3 and Experiment 7 were also different.

As it can be seen from Table 5, although the effect of the voltage on the average fiber diameter was not significant. However, the voltage had a great influence on P1, P2, and P3. Therefore, if we want to achieve the effect of changing the porosity of each layer without significantly affecting the fiber diameter, adjusting the voltage was a good method.

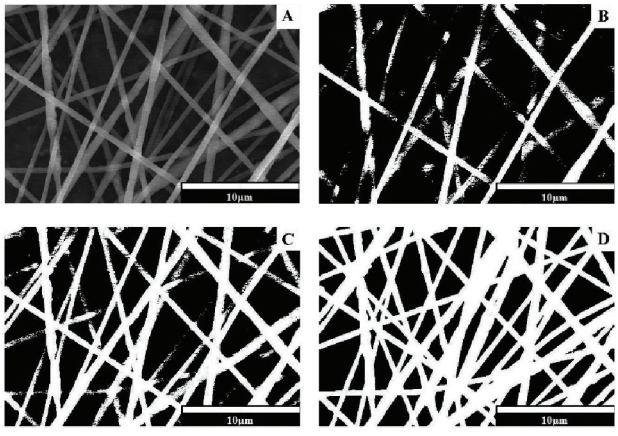

Figure 7: Binary image with different thresholds for Experiment 7 sample: (a) original image, (b) binary image with threshold 1, (c) binary image with threshold 2 and (d) binary image with threshold 3.

It is well known that the porosity of scaffolds is an important parameter in many tissue engineering applications. Appropriate porosity and pore morphology provide space for growth of blood vessels and migration of cells and ensure efficient exchange of waste products and nutrients between cells and their microenvironment. The following is the Jain et al.'s description of the different functions of different layers' porosity: The decreasing porosity from the top surface toward the substrate suggests that while top layer would provide support for cell proliferation and growth, the subsequent layers with sufficient but lower porosity will allow transport of nutrient, blood, and waste (30). It can be seen that proper porosity of various layer is very important for cell growth. Therefore, using the conclusions of this paper, the porosity of each layer can be adjusted to prepare the CSBS nanofiber web suitable for cell growth and proliferation. For the first time, this paper used orthogonal experiments to study the effects of CSBS process parameters on the porosity of different layers of nanofiber web. These conclusions can promote the applications of the CSBS method in tissue engineering, bioengineering, filtration engineering and so on.

The porosity of nanofiber webs produced by electrospinning (ES) and CSBS technology was also compared. The process parameters and porosity of the electrospinning and CSBS were shown in Table 6. In each experiment, inner diameter of the needle (0.42 mm) and solution concentration (7%) were kept constant. The injection rates were kept constant in Experiments 1-4 (0.2 ml/h), and the injection rates of Experiments 5 and 6 were the same (0.5 ml/h). It can be seen from Table 6 that the nanofiber membranes obtained by the two spinning methods have similar porosity.

Table 6: Comparison of porosity between electrospinning and CSBS.

No.	Spinning system	Injection rate (ml/h)	P1 (%)	P2 (%)	P3 (%)	Voltage (kV)	Air pressure (MPa)	Distance parameter (cm)
1	ES	0.2	87.0132	76.5018	71.2015	14	——	SD=55
2	CSBS	0.2	85.1415	75.46625	70.08875	7	0.015	LC=14; DC=15 NCD=15; CCD=95
3	ES	0.2	75.3965	66.01786	59.521	14	——	SD=45
4	CSBS	0.2	76.31075	66.30825	61.27975	10	0.01	LC=14; DC=20 NCD=15; CCD=85
5	ES	0.5	78.3698	68.32484	62.4938	13	——	SD=40
6	CSBS	0.5	76.39874	66.03654	61.332	10	0.01	LC=8; DC=15 NCD=5; CCD=95

4 Conclusions

Firstly, the effects of NCD, LC, and CCD on the diameter of CSBS nanofiber were evaluated. We found that decreasing NCD or increasing LC can reduce the nanofiber diameter, the CCD didn't significantly affect the diameter of nanofibers. Furthermore, the orthogonal array design method was adopted to study the effects of the injection rate, air pressure, NCD, LC, DC, voltage and CCD on the fiber average diameter, diameter standard deviation and porosity of various layers (P1, P2, and P3). The influence order of each process parameter on the above properties of nanofiber web was found, and the corresponding optimal spinning process parameters were listed. Finally, we have also found that by adjusting the voltage, the porosity of each layer can be significantly changed without causing a significant change in CSBS nanofiber diameter.

This work first investigated the effects of CSBS process parameters on the fiber diameter and porosity of various layers. It is well known that fiber diameter and porosity of nanofiber webs were important parameters in tissue engineering, bioengineering, filtration engineering and other applications. The conclusions of this article can help researchers to produce high quality CSBS nanofiber and promote the wider application of this novel technology.

Acknowledgments: This study was supported by the National Natural Science Foundation of China (51776034).

References

1. Medeiros E.S., Glenn G.M., Klamczynski A.P., Orts W.J., Mattoso L.H.C., Solution blow spinning: A new method to produce micro- and nanofibers from polymer solutions. J Appl Polym Sci, 2009, 113, 2322-2330.
2. Tutak W., Sarkar S., Lin-Gibson S., Farooque T.M., Jyotsnendu G., Wang D., et al., The support of bone marrow stromal cell differentiation by airbrushed nanofiber scaffolds. Biomaterials, 2013, 34, 2389-2398.
3. Polat Y., Pampal E.S., Stojanovska E., Simsek R., Hassanin A., Kilic A., et al., Solution blowing of thermoplastic polyurethane nanofibers: A facile method to produce flexible porous materials. J Appl Polym Sci, 2016, 133.
4. Bilbao-Sainz C., Chiou B.-S., Valenzuela-Medina D., Du W.-X., Gregorski K.S., Williams T.G., et al., Solution blow spun poly(lactic acid)/hydroxypropyl methylcellulose nanofibers with antimicrobial properties. Eur Polym J, 2014, 54, 1-10.
5. Abdal-hay A., Sheikh F.A., Lim J.K., Air jet spinning of hydroxyapatite/poly(lactic acid) hybrid nanocomposite membrane mats for bone tissue engineering. Colloids Surf B Biointerfaces, 2013, 102, 635-643.
6. Behrens A.M., Casey B.J., Sikorski M.J., Wu K.L., Tutak W., Sandler A.D., et al., In Situ Deposition of PLGA Nanofibers via Solution Blow Spinning. ACS Macro Letters, 2014, 3, 249-254.
7. Tao X., Zhou G., Zhuang X., Cheng B., Li X., Li H., Solution blowing of activated carbon nanofibers for phenol adsorption. RSC Advances, 2015, 5, 5801-5808.
8. Hsiao H.-Y., Huang C.-M., Hsu M.-Y., Chen H., Preparation of high-surface-area PAN-based activated carbon by solution-blowing process for CO2 adsorption. Sep Purif Technol, 2011, 82, 19-27.
9. Wang H., Zhuang X., Li X., Wang W., Wang Y., Cheng B., Solution blown sulfonated poly(ether sulfone)/poly(ether sulfone) nanofiber-Nafion composite membranes for proton exchange membrane fuel cells. J Appl Polym Sci, 2015, 132.
10. Xu X., Li L., Wang H., Li X., Zhuang X., Solution blown sulfonated poly(ether ether ketone) nanofiber–Nafion composite membranes for proton exchange membrane fuel cells. RSC Advances, 2015, 5, 4934-4940.
11. Jia K., Zhuang X., Cheng B., Shi S., Shi Z., Zhang B., Solution blown aligned carbon nanofiber yarn as supercapacitor electrode. J Mat Sci-Mater El, 2013, 24, 4769-4773.
12. Zhuang X., Jia K., Cheng B., Feng X., Shi S., Zhang B., Solution blowing of continuous carbon nanofiber yarn and its electrochemical performance for supercapacitors. Chem Eng J, 2014, 237, 308-311.
13. Shi S., Zhuang X., Cheng B., Wang X., Solution blowing of ZnO nanoflake-encapsulated carbon nanofibers as electrodes for supercapacitors. J Mat Chem A, 2013, 1, 13779.
14. Chen S., Hou H., Harnisch F., Patil S.A., Carmona-Martinez A.A., Agarwal S., et al., Electrospun and solution blown three-dimensional carbon fiber nonwovens for application as electrodes in microbial fuel cells. Energy Environ Sci, 2011, 4, 1417.
15. da Silva Parize D.D., Foschini M.M., de Oliveira J.E., Klamczynski A.P., Glenn G.M., et al., Solution blow spinning: parameters optimization and effects on the properties of nanofibers from poly(lactic acid)/dimethyl carbonate solutions. JMatS, 2016, 51, 4627-4638.
16. Li L., Kang W., Zhuang X., Shi J., Zhao Y., Cheng B., A comparative study of alumina fibers prepared by electro-blown spinning (EBS) and solution blowing spinning (SBS). Mater Lett, 2015, 160, 533-536.
17. Zheng W., Zheng W., Shi C., Wang X., Cylindrical-electrode-assisted solution blowing for nanofiber spinning. J Appl Polym Sci, 2019, 136, 47087.
18. Jiang S., Chen Y., Duan G., Mei C., Greiner A., Agarwal S., Electrospun nanofiber reinforced composites: a review. Polym Chem-UK, 2018, 9, 2685-2720.
19. Schiffman J.D., Schauer C.L., A Review: Electrospinning of Biopolymer Nanofibers and their Applications. Polym Rev, 2008, 48, 317-352.
20. Greiner A., Wendorff J.H., Electrospinning: a fascinating method for the preparation of ultrathin fibers. Angew Chem Int Ed Engl, 2007, 46, 5670-5703.
21. Ghasemi-Mobarakeh L., Semnani D., Morshed M., A novel method for porosity measurement of various surface layers of nanofibers mat using image analysis for tissue engineering applications. J Appl Polym Sci, 2007, 106, 2536-2542.
22. Doshi J., Reneker D.H., Electrospinning process and applications of electrospun fibers. J Electrostatics, 1995, 35, 151-160.

23. Bolbasov E.N., Stankevich K.S., Sudarev E.A., Bouznik V.M., Kudryavtseva V.L., Antonova L.V., et al., The investigation of the production method influence on the structure and properties of the ferroelectric nonwoven materials based on vinylidene fluoride – tetrafluoroethylene copolymer. Mater Chem Phys, 2016, 182, 338-346.
24. Sinha-Ray S., Sinha-Ray S., Yarin A.L., Pourdeyhimi B., Theoretical and experimental investigation of physical mechanisms responsible for polymer nanofiber formation in solution blowing. Polymer, 2015, 56, 452-463.
25. Ki C.S., Baek D.H., Gang K.D., Lee K.H., Um I.C., Park Y.H., Characterization of gelatin nanofiber prepared from gelatin–formic acid solution. Polymer, 2005, 46, 5094-5102.
26. Daristotle J.L., Behrens A.M., Sandler A.D., Kofinas P., A Review of the Fundamental Principles and Applications of Solution Blow Spinning. ACS Appl Mater Interfaces, 2016, 8, 34951-34963.
27. Cheng B., Tao X., Shi L., Yan G., Zhuang X., Fabrication of ZrO2 ceramic fiber mats by solution blowing process. Ceram Int, 2014, 40, 15013-15018.
28. Tan E.P., Ng S.Y., Lim C.T., Tensile testing of a single ultrafine polymeric fiber. Biomaterials, 2005, 26, 1453-1456.
29. Gholipourmalekabadi M., Mozafari M., Bandehpour M., Salehi M., Sameni M., Caicedo H.H., et al., Optimization of nanofibrous silk fibroin scaffold as a delivery system for bone marrow adherent cells: in vitro and in vivo studies. Biotechnol Appl Biochem, 2015, 62, 785-794.
30. Jain S., Sharma A., Basu B., In vitro cytocompatibility assessment of amorphous carbon structures using neuroblastoma and Schwann cells. J Biomed Mater Res B Appl Biomater, 2013, 101, 520-531.